Initial Development of Noncircular Jets Leading to Axis Switching

Shozo Koshigoe,* Ephraim Gutmark,† and Klaus C. Schadow‡
Naval Weapons Center, China Lake, California
and
Arnold Tubis*
Purdue University, West Lafayette, Indiana

This paper discusses the underlying mechanisms for the deformation of coherent structures which occurs in the initial stage of the axis switching of noncircular jets. The generalized shooting method is applied to jets with elliptic-core and equilateral-triangular-core regions of constant flow. The analysis reveals that in order to have the deformation, three requirements must be present in the behavior of the eigenmodes of noncircular jets: 1) the eigenfunctions are localized without excessive overlapping; 2) the amplification rates of the corresponding eigenmodes are comparable; and 3) sufficient phase speed difference exists between the eigenmodes. The qualitative behavior of the noncircular jets found through the numerical analysis is compared with experimental results and are in good correlation with them.

I. Introduction

ONE of the most peculiar aspects of noncircular jet evolution[1-5] is axis switching, which is of interest from a fundamental scientific point of view and for its potential application.[6] We have investigated the initial development of axis switching in the elliptic-core jet through the use of instability analysis.[7] The initial development of axis switching is characterized by the deformation of the coherent structures in the elliptic jet. The deformation of the structures and subsequent development of axis switching can be associated with the self-induction of the asymmetrical distribution of the vorticity in the elliptic jet,[8] which causes differences in roll-up locations. The portions of the elliptic vortical structure around the major axis roll up slightly farther downstream than those of the minor axis. Thus, the rolled-up structure in elliptic shape appears to be deformed. This deformation of the elliptic jet is clearly seen in the forced elliptic jets in Ho and Gutmark's paper[9] (see Fig. 10). The deformation is the initial development in the axis switching of the jet. The analysis for the axis switching of the jet is beyond the scope of the present work. However, it must be pointed out that, without the deformation in the initial development, there will be no switching of the axis for the jet.

Flowfield measurements show that an equilateral-triangular jet also undergoes a switch in its shape orientation in the downstream direction.[10] The spreading rate of the flow at the flat sides is larger than at the vertices. The amplification of turbulence is different at the two sections, and so is the turbulence structure.[11] Coherent structures are generated at the triangle's flat side, but fine-scale turbulence dominates the flow emanating from the vertices. This observation has also been confirmed in reacting triangular flames.[12]

The coexistence of large-scale structures at the flat sides and small-scale eddies at the vertices makes the triangular jet an attractive flow configuration for combustion systems.[13] The unique combination of large- and fine-scale mixing of the combustion reactants and the molecular mixing is necessary for the chemical reaction.

In this paper, we analyze the equilateral-triangular-core jet in terms of the behavior of eigenmodes. The results are compared with those of the elliptic-core jet in order to demonstrate the common underlying mechanisms of the deformation in the noncircular jets from the perspective of instability analysis. The generalized shooting method,[14] based on both integral and differential equations, is used for the calculations because it has been found to be more practical to apply than the Helmholtz integral equation formation.[15]

The assumed symmetry properties and the associated spatial instability classes of triangular jets are given in Sec. II, and the analytic specification of the jet mean flow profile and coordinate transformation of the Rayleigh equation are presented in Sec. III. The numerical results for the behavior of the eigenmodes in triangular-core jet are compared with those of elliptic-core jets to demonstrate the common mechanisms of the deformation of noncircular jets. The qualitative comparison between numerical and experimental results are made with respect to the underlying mechanisms for the deformation of noncircular jets in Sec. IV.

II. Assumed Symmetry Properties and Spatial Instability Classes of Triangular-Core Jets

We express the velocity profile of a straight jet in an inviscid incompressible fluid with incremental pressure p and density ρ as

$$U = W(x,y)\hat{e}_z + \boldsymbol{u} \tag{1}$$

where $W\hat{e}_z$ is the jet mean flow velocity ($W>0$) and $\boldsymbol{u}$ the fluctuating velocity associated with spatial instabilities. Application of the linearized momentum and mass-conservation equations and the assumed (z,t) dependence, $\exp\{i(\alpha z-\omega t)\}$ for $\boldsymbol{u}$, p, and ρ, then gives the Rayleigh equation

$$(\nabla^2-\alpha^2)p+[2\alpha/(\omega-\alpha W)]\,\nabla W\cdot\nabla p=0 \tag{2}$$

Presented as Paper 88-0037 at the AIAA 26th Aerospace Sciences Meeting, Reno, NV, Jan. 11-14, 1988; received Jan. 26, 1988; revision received April 25, 1988.

*Physicist, Research Department. Member AIAA.

†Aerospace Engineer, Research Department. Member AIAA.

‡Supervisory General Engineer, Research Department.

§Professor, Department of Physics.

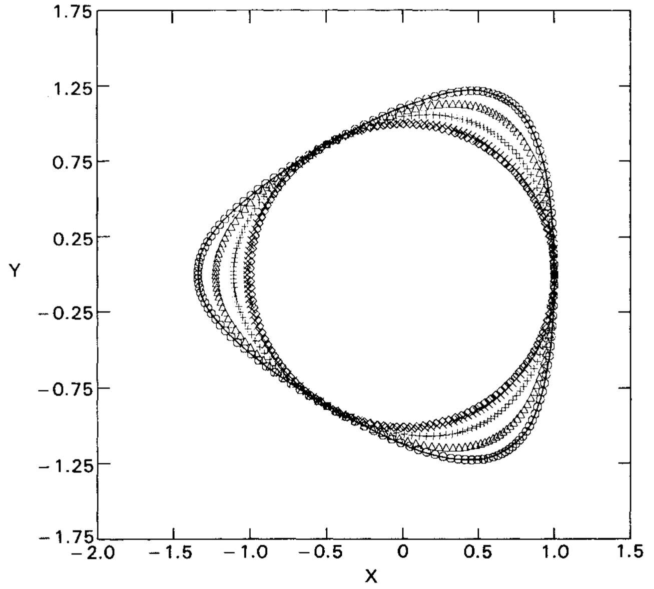

Fig. 1 $W=0.5$ **contours from inside (diamond-shaped) to outside (circular-shaped) with** $a_2=0$, **0.5, 1, 1.5, and 2. The solid line represents measured contours at** $z/D_e=0.2$, **where** z **is the streamwise distance from the nozzle, and** D_e **is the equivalent nozzle diameter.**

where

$$\nabla=\hat{e}_x\frac{\partial}{\partial x}+\hat{e}_y\frac{\partial}{\partial y}$$

For a given frequency ω, the solution of Eq. (2) with p finite and $\rightarrow 0$ for $r=\sqrt{x^2+y^2}\rightarrow\infty$ yields the corresponding wave number $(Re\{\alpha\}=\alpha_r)$ and spatial growth rate $(-\mathrm{Im}\{\alpha\}=-\alpha_i)$.

On the basis of mean flow data for triangular jets shown as the solid line in Fig. 1 (see Sec. III for details), we assume that the mean flow W, expressed as a function of the polar coordinates (r,ϕ), has the symmetry properties

$$W(r,\phi)=W(r,-\phi) \qquad W(r,\phi)=W(r,\phi+2\pi/3) \tag{3}$$

in addition to the single-valuedness condition

$$W(r,\phi\pm 2\pi)=W(r,\phi) \tag{4}$$

It then follows from Eqs. (2-4) that a formal group theoretic argument[16] shows that there are four symmetry classes of eigenfunctions.

Class 1: $c_{3\ell}(\ell=0,1,2,\ldots)$

$$p_c^{(3\ell)}(r,\phi+2\pi/3)=p_c^{(3\ell)}(r,\phi) \tag{5a}$$

$$p_c^{(3\ell)}(r,\phi)=p_c^{(3\ell)}(r,-\phi) \tag{5b}$$

$$p_c^{(3\ell)}(r,\phi)=\sum_{n=0}^{\infty}A_{3n}^{(3\ell)}(r)\cos(3n\phi) \tag{5c}$$

Class 2: $s_{3\ell}(\ell=1,2,3,\ldots)$

$$p_s^{(3\ell)}(r,\phi+2\pi/3)=p_s^{(3\ell)}(r,\phi) \tag{6a}$$

$$p_s^{(3\ell)}(r,\phi)=-p_s^{(3\ell)}(r,-\phi) \tag{6b}$$

$$p_s^{(3\ell)}(r,\phi)=\sum_{n=1}^{\infty}B_{3n}^{(3\ell)}(r)\sin(3n\phi) \tag{6c}$$

Classes 3 and 4: $e_{3\ell\pm 1}(\ell=0,1,2,\ldots)$

$$p_e^{(3\ell\pm 1)}(r,\phi+2\pi/3)=e^{\pm i2\pi/3}p_e^{(3\ell\pm 1)}(\phi) \tag{7a}$$

$$p_e^{(3\ell\pm 1)}(r,\phi)=p_e^{(3\ell\pm 1)}(r,-\phi) \tag{7b}$$

$$p_e^{(3\ell\pm 1)}(r,\phi)=\sum_{n=-\infty}^{\infty}C_{3n\pm 1}^{(3\ell\pm 1)}(r)e^{i(3n\pm 1)\phi}$$

$$C_{3n\pm 1}^{(3\ell\pm 1)}=C_{3(-n)\mp 1}^{(3\ell\mp 1)} \tag{7c}$$

The $c_{3\ell}$ and $s_{3\ell}$ eigenmodes correspond to one-dimensional representations of the group of proper covering operations of an equilateral triangle, whereas the $e_{3\ell\pm 1}$ eigenmodes correspond to the two-dimensional representation of this group (see, e.g., page 8 of Ref. 16). An analogous classification of elliptic jet eigenmodes has been given by Morris[17] and the present authors.[14,15]

The symmetry properties given in Eqs. (5-7) allow the computation region to be limited to $0\leq\phi\leq\pi/3$ for $c_{3\ell}$ and $s_{3\ell}$ and $|\phi|\leq\pi/3$ for $e_{3\ell\pm 1}$. Because we are interested in an in-phase forced jet, we will discuss only the eigenmode class $c_{3\ell}$ in the following.

III. Specification of the Mean Flow and Coordinate Transformation of the Rayleigh Equation

The core region of uniform mean flow is assumed to be bounded by the equilaterial triangle shown in Fig. 1. We will use the nondimensionalized coordinates

$$x=x^*/L, \qquad y=y^*/L \tag{8}$$

where x^*, y^* are the unscaled coordinates, and $L=2\times$ the triangle area bounded by half the mean velocity contour/circumference of the same triangle.

It is convenient to represent equal-mean-velocity contours by the family of closed curves (the so-called Toda equipotential curves)[18]

$$H(x,y)=\exp\{-(a_2/2)(x+\sqrt{3}y)\}+\exp\{-(a_2/2)(x-\sqrt{3}y)\}$$
$$+\exp(a_2x)+\sqrt{x^2+y^2}=a_3 \tag{9}$$

with a_2 fixed and a_3 an implicit function of the mean velocity, given by $a_3=H(x_0,0)$. The parameter x_0 is related to the mean velocity $W(w,y)$ (nondimensionalized by the core region velocity W_0) by

$$W(x_0,0)=\frac{1}{2}\left[1-\tanh\left(\frac{x_0-1}{2\theta_0}\right)\right] \tag{10}$$

where θ_0 is the momentum thickness (chosen to be 0.02). The typical mean velocity contours [$W=0.5$ or $x_0=1$ from Eq. (10), from which a_3 can be determined; thus, the mean velocity contours are obtained by Eq. (9)] for various a_2 and a measured velocity contour are shown in Fig. 1. For the fixed $a_2=2$, two mean-velocity contours C and $\bar{C}$ corresponding to $W=10^{-6}$ and $1-10^6$, respectively (see Fig. 2), are found through Eq. (9) for two different values of a_3 (remember that a_3 is a function of W). Note that the modification of the mean-velocity contours from the triangular shape to, e.g., a rectangular shape can be easily achieved by adding one more exponential term and replacing the respective exponents with appropriate angle relations in Eq. (9).

The core region, with $W=W_0$ const, is bounded by the triangle (C) shown in Fig. 2. The Cartesian coordinates $(x_e,$

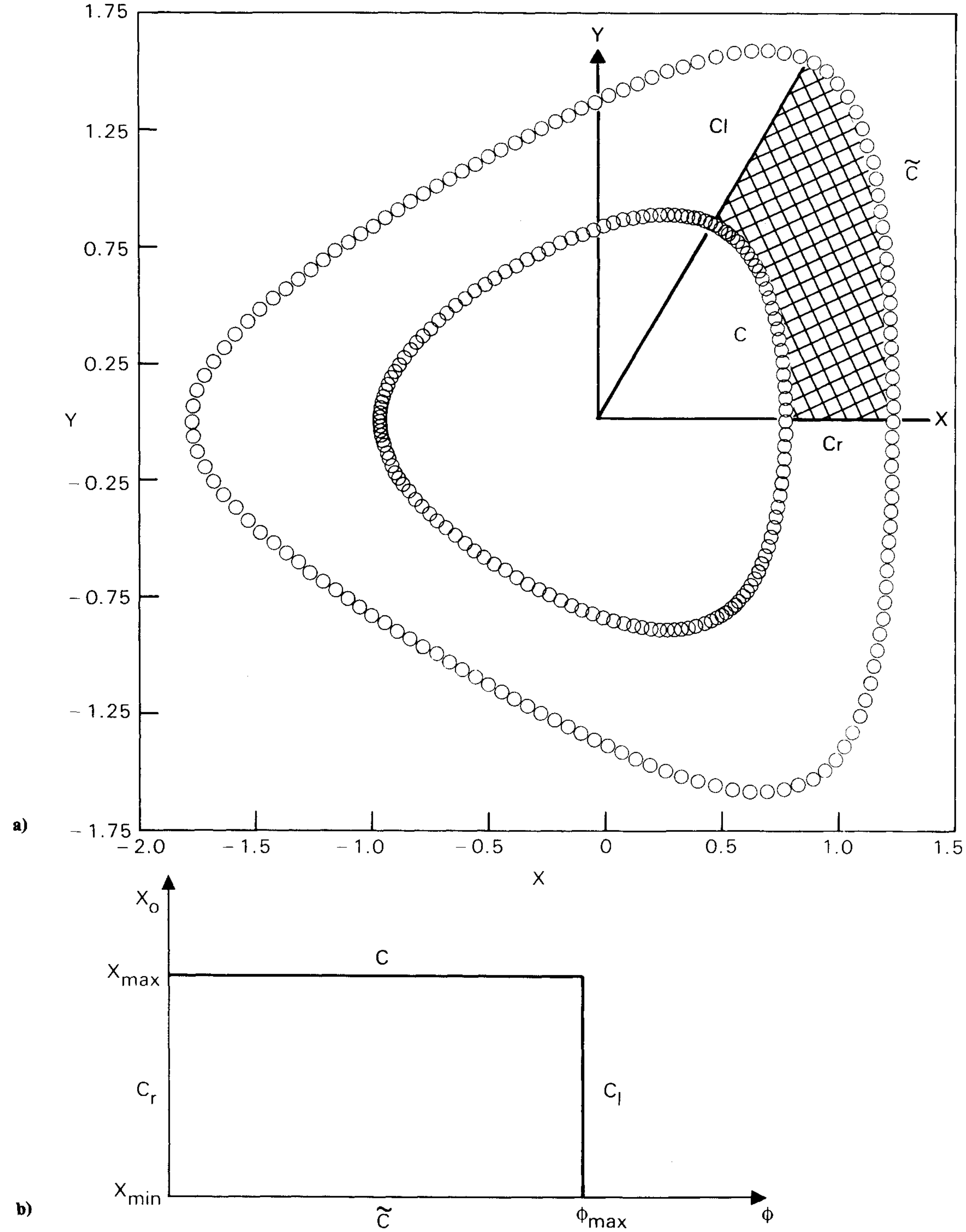

Fig. 2 Node points on the contours for $W = W_1 = 10^{-6}(C)$ and $W = W_N = 1 - 10^{-6}$ ($\tilde{C}$, for $\theta_0 = 0.02$, $a_2 = 2$, and $\sigma = 1$); a) the actual calculation region is cross-hatched, and b) the transformed calculation region is in the x_0 and ϕ plane.

y_e) of a point on this triangle are related through

$$y_e = (a_2 \sigma \phi + \tan\phi) x_e \tag{11}$$

where ϕ is the polar angle, defined as $0 \le \phi \le \phi_{\max}$, with $\phi_{\max}$ given by

$$a_2 \sigma \phi_{\max} + \tan\phi_{\max} = \sqrt{3} \tag{12}$$

and σ is a parameter that controls the node distribution on C. A given point $\boldsymbol{x} = (x,y)$ outside this triangle is then specified as the intersection of the normal line to the point (x_e, y_e) on C and the contour described by Eq. (9). Thus, x and y are functions of x_0 and ϕ. The momentum thickness distribution described earlier (see Fig. 2) will be called NU1 (nonuniform).

For the triangular-core jet (the contour of the core is represented by the curve C, which is found by the same way as earlier) with equimomentum thickness, the contours outside of C are specified by W, where

$$W(x,y) = \frac{1}{2}\left[1 - \tanh\left(\frac{x_0(x,y) - 1}{2\theta_0}\right)\right] \tag{13}$$

where x_0 is the distance measured from a point (x_e, y_e) on C along the normal line. We shall use the abbreviation U1

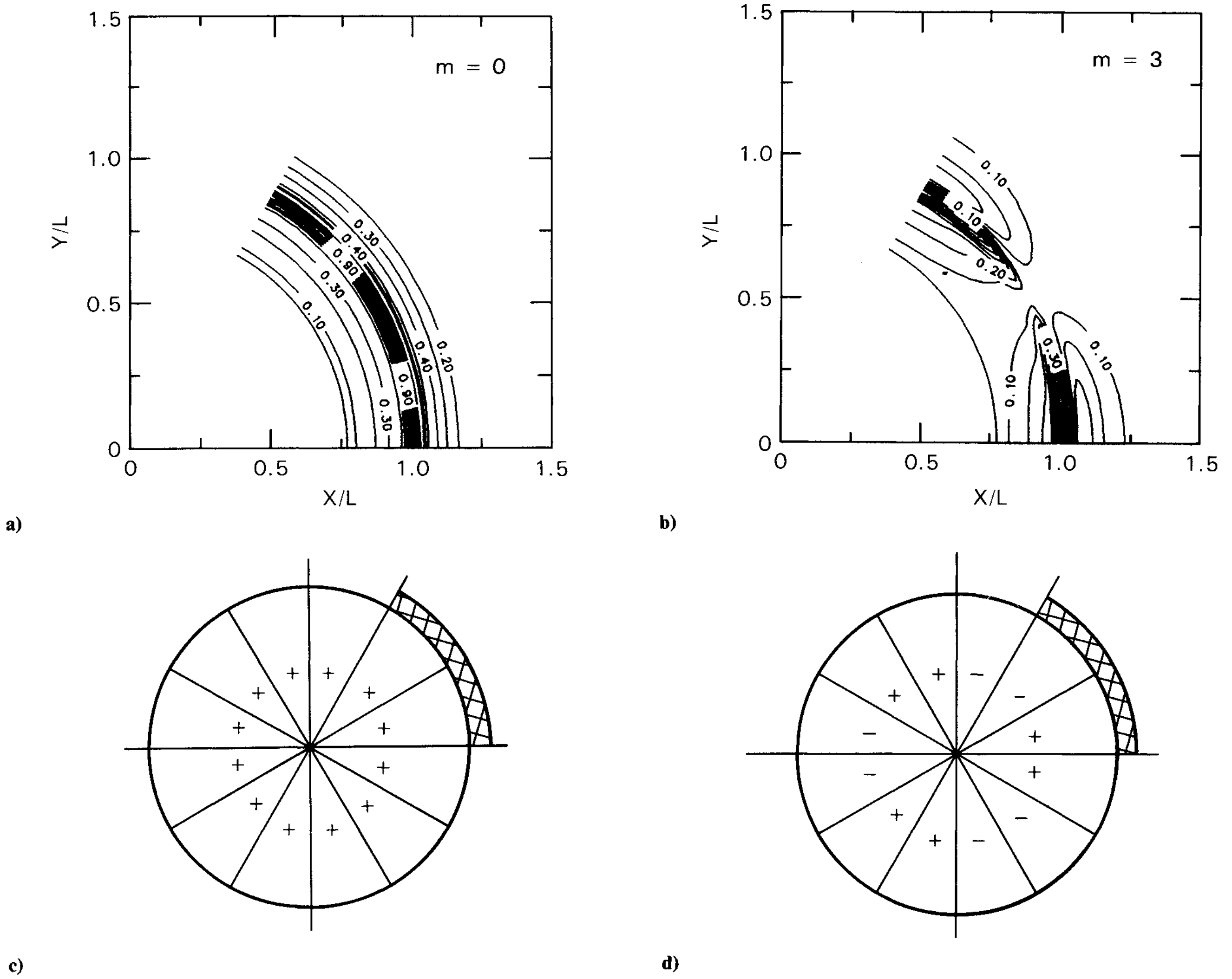

Fig. 3 Contour plots of $|u_z|$ of circular-jet modes at $\omega = 5.4$ [with cos$m\phi$, $m = 0$, a); $m = 3$, c); azimuthal variations] and their corresponding schematic azimuthal phase variations b) and d), respectively.

(uniform) for this type of momentum thickness distribution.

It will be convenient to make a transformation of variables from x,y to x_0,ϕ [defined in Eqs. (10–13), respectively]. A relation between x,y, and x_0,ϕ is easily found from Eqs. (9–13) and the expression for the normal line to C.

The transformed Rayleigh equation, Eq. (2), may be obtained in the form

$$\frac{\partial^2 p}{\partial x_0^2}+b_1\frac{\partial^2 p}{\partial \phi^2}+2b_2\frac{\partial^2 p}{\partial \phi \partial x_0}-b_3 p+b_4\frac{\partial p}{\partial x_0}+b_5\frac{\partial p}{\partial \phi}=0 \tag{14}$$

where the b_i are functions of α, ω, x_0, and ϕ. The transformation of the computation region is shown in Fig. 2. The x_0-ϕ plane node points for the finite-difference calculations are

$$\phi_i=\frac{\phi_{\max}}{M-1}(i-1), \qquad i=1,2,\ldots,M$$

$$x_0=\frac{x_{\max}-x_{\min}}{N-1}(j-1), \qquad j=1,2,\ldots,N \tag{15}$$

where $x_{\min}$ and $x_{\min}$ are found through Eqs. (10) and (13) corresponding to $W_1=10^{-6}$ and $W_n=1-W_1$, respectively. In our calculations, $\theta_0 = 0.02$, $M = 25$, and $N = 215$, unless otherwise indicated.

IV. Discussion

The numerical results are presented for the fundamental and first "overtone" of the $c_{3\ell}$ class [Eqs. (5a–c)] with two types of azimuthal momentum thickness distribution (NU1 and U1). The calculational results are compared with the behaviors of eigenmodes in elliptic-core jet. The common features in eigenmodes of triangular- and elliptic-core jets are discussed in relation to the underlying mechanisms of the deformation of the coherent structures in the noncircular jets.

The modal fluctuation velocity components are related to the pressure eigenfunction by

$$u_x=\frac{1}{i\rho_0(\omega-\alpha W)}\frac{\partial p}{\partial x} \tag{16a}$$

$$u_y=\frac{1}{i\rho_0(\omega-\alpha W)}\frac{\partial p}{\partial y} \tag{16b}$$

$$u_z=\frac{1}{\rho_0(\omega-\alpha W)}\left[\alpha p-\frac{1}{(\omega-\alpha W)}\times\left(\frac{\partial p}{\partial x}\frac{\partial W}{\partial x}+\frac{\partial p}{\partial y}\frac{\partial W}{\partial y}\right)\right] \tag{16c}$$

where ρ_0 is the ambient density.

In Fig. 3, contour plots are shown for the magnitude $|u_z|$ of circular-jet modes at approximately the frequency ($\omega = 5.4$) of maximal amplification [with $\cos m\phi$, $m = 0$ (a); $m = 3$ (c), azimuthal variations] and their schematic azimuthal phase variations (b) and (d), respectively. The magnitude and phase ϕ_z of u_z are defined by

$$u_z = |u_z| e^{i\phi_z} \tag{17}$$

It is clear from Eqs. (5c) and (6c) that the circular-jet modes, $m = 0$ and $m = 3$, are special cases of $p_c^{(0)}$ and $p_c^{(3)}$ [or $p_s^{(3)}$].

Now the circular mean-velocity profile is deformed into triangular profiles by increasing the value for a_2 (see Fig. 1). The frequency is kept at $\omega = 5.4$, which corresponds approximately to the most amplified frequency. Two types of azimuthal momentum thickness distribution are studied. The first is typically found in the initial development region of the triangular-core jet, where the momentum thickness at the vertex is larger than that at the flat side (see Fig. 2). The second one is an equimomentum thickess distribution. We have assigned the abbreviations NU1 and U1 for the first and second types of momentum thickness distributions, respectively. There is no difference between NU1 and U1 at the limit of $a_2 = 0$ (see Fig. 3). The mean-velocity contours are now deformed from the circular to triangular shape by increasing a_2. Figure 4 shows the magnitude $|u_z|$ of c_0 [NU1 (a) and U1 (c)] and c_3 [NU1 (b) and U1 (d)] eigenmodes for $a_2 = 2$. The eigenfunctions c_0 and c_3 for NU1 both show negligible activities at the vertex. Maximum activities occur at $\phi = 0$ for this case, and they are always scaled as one. The increased activities of $|u_z|$ for both eigenmodes around the flat side are evident. This implies that in the initial development region of the triangular jet, the coherent structures are found only around the flat side. On the other hand, the maximum activity of eigenfuction c_3 is now shifted to the vertex for U1. With this coexistence of eigenmodes c_0 and c_3, it is possible to find the coherent structures at all azimuthal locations of the triangular-core jet for U1. The behavior of the corresponding eigenvalues is depicted in Fig. 5 as a_2 is increased from 0 to 2. For NU1, the amplification rates for c_3 are rapidly decreased relative to those of c_0 as a_2 are increased. There is a minute phase-speed (C_p) difference between modes for $a_2 = 2$. The eigenvalues for U1 show strikingly different behavior from those for NU1. There is no significant depression in the amplification rate for the c_3 mode. The amplification rates for c_0 and c_3 modes are comparable. There is a noticeable difference in the phase speed between c_0 and c_3 modes as a_2 is increased. The phase speed of c_3 is increased, whereas that of c_0 is decreased with increasing a_2. The amplification rates and phase speeds (C_p) of the eigenmodes c_0 and c_3 for two types of momentum thickness distribution (NU1 and U1) are shown as functions of ω in Fig. 6. The differences in the amplification rates for the eigenmodes c_0 and c_3 with NU1 are significantly larger than those of the same eigenmodes with U1, regardless of the frequencies. The phase speed of the c_3 mode is consistently higher than that of the c_0 mode for all of the calculated frequencies in the case of U1. The absolute differences in the phase speeds between the two modes are especially greater in the case of U1 than in that of NU1 in the vicinity of the most amplified frequency. Therefore, it is apparent that selection of frequency (e.g., choice of 5 or 6 for ω) does not alter the behavior of the two modes described in Fig. 5.

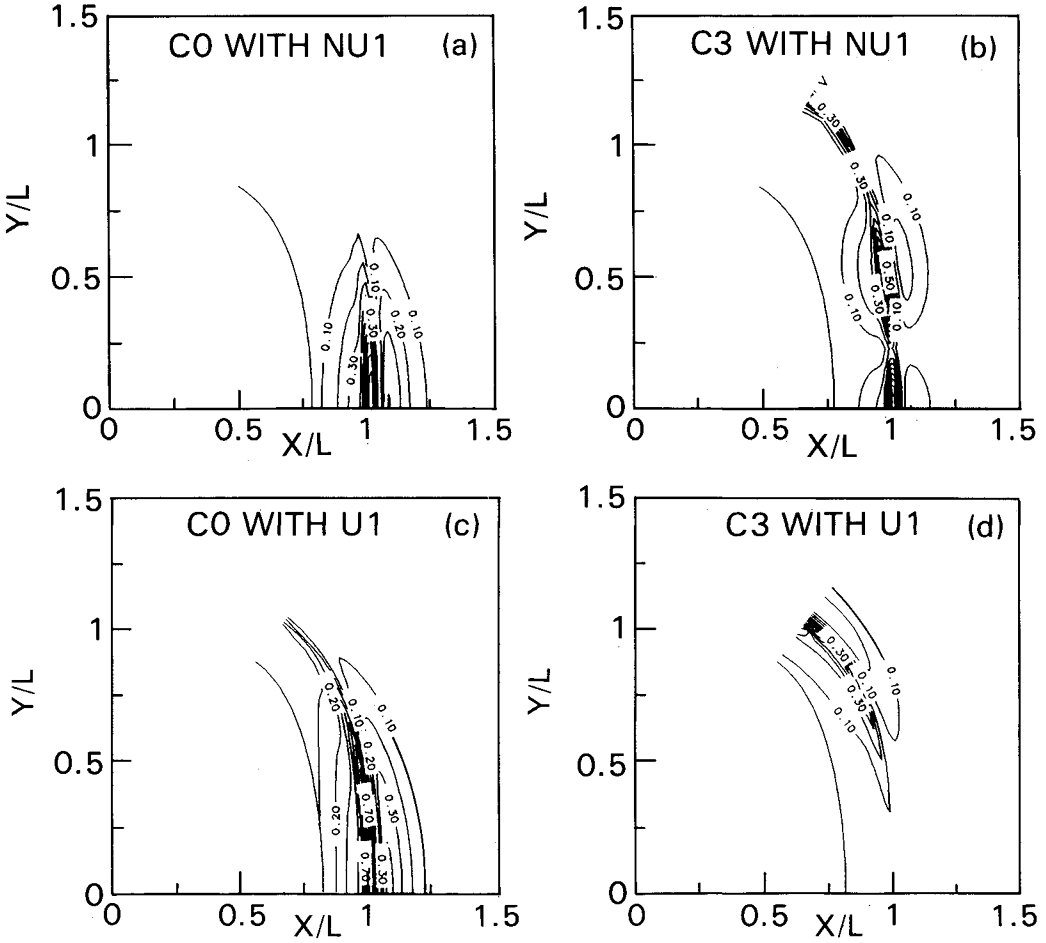

Fig. 4 Contour plots of $|u_z|$ of eigenfunctions, at $\omega = 5.4$ for $a_2 = 2$.

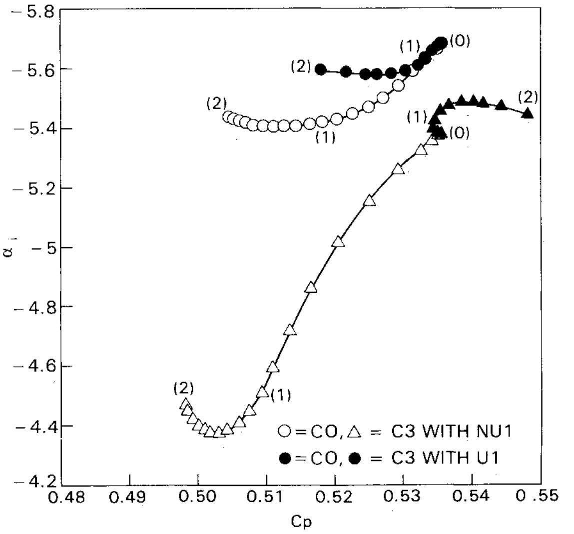

Fig. 5 The evolution of eigenvalues at $\omega = 5.4$ in α_i and C_p plane for eigenmodes, as a_2 is varied from 0 to 2. The number in (N) indicates the value of a_2.

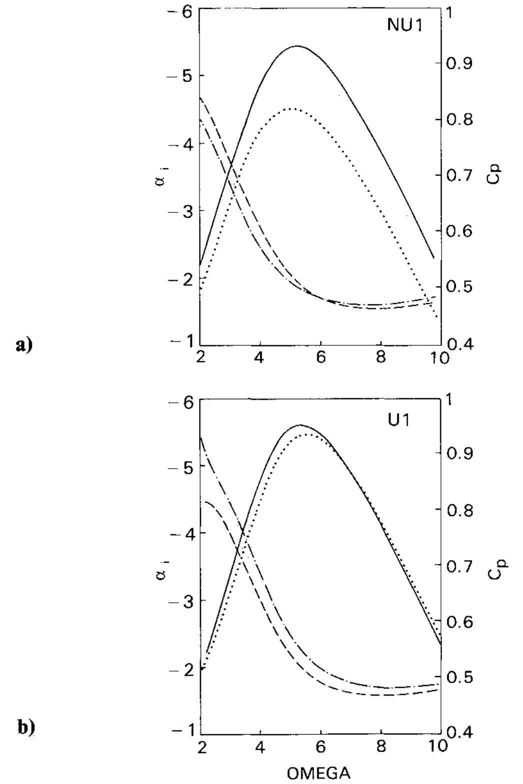

Fig. 6 α_i (solid line for c_0 and dotted line for c_3) and C_p (dashed line for c_0 and chain-dotted line for c_3) are shown as functions of ω for $a_2 = 2$ with a) NU1 and b) U1.

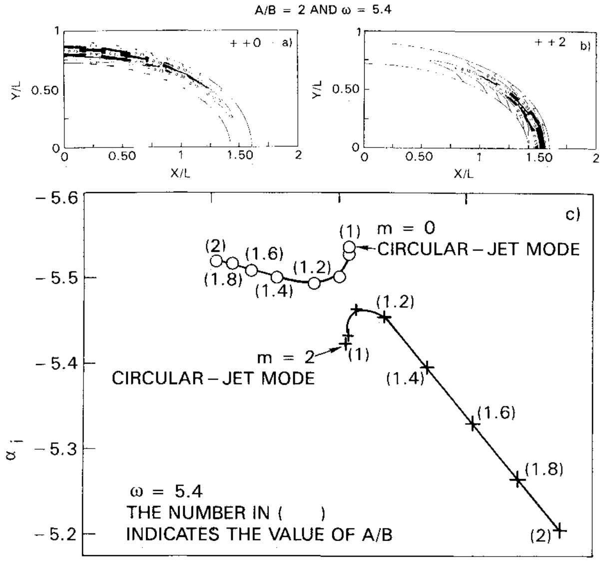

Fig. 7 Contour plots of $|u_z|$ of eigenfunctions, a) and b); and the evolution of eigenvalues in α_i and C_p plane for eigenmodes, c).

Two significantly different aspects for the behavior of the triangular-core jets are found, depending on the types of azimuthal momentum thickness distribution NU1 and U1. The first aspect relating to the behavior of eigenmodes with NU1 is that, as a_2 is increased, the eigenmodes c_0 and c_3 show negligible activities at the vertex with increased activities around the flat side, and the amplification rates for c_3 are greatly depressed in comparison to those of c_0 with an insignificant difference in phase speeds between the two modes. The second one, which is associated with U1, is that the activities of the eigenmodes are polarized; the maximum activity of the c_0 mode is concentrated around the flat side, whereas that of the c_3 modes is localized at the vertex of the triangular-core jet, and a noticeable phase-speed difference is created without loss of a comparable amplification rate between two modes. The first aspect is inherent in the initial development region of the jets issued from nozzles containing sections with acute corners. The discussion of the second aspect will be carried out by comparison with similar behavior found in the elliptic-core jets.

The initial development of the axis switching of elliptic-core jet is studied through the behavior of the eigenmodes. The evolution of the two circular-jet modes $m = 0$ and 2 is examined as eccentricity is increased. The azimuthal distribution of momentum thickness is kept uniform [chosen to be 0.02 of $L = \sqrt{(AB)}$] and $A/B = 2$ (A and B are lengths of semimajor and semiminor axes, respectively) is assumed unless stated differently. As the eccentricity of the jet is increased, the eigenfunctions become localized [one that evolved from $m = 0$ circular-jet mode $(+ +0)$ is localized around the minor axis, and the other one evolved from $m = 2$ circular-jet mode $(+ +2)$ is around the major axis], as shown in Figs. 7a and 7b. Phase-speed differences increase between the two eigenmodes as the eccentricity increases, while the comparable amplification rates are maintained as shown in Fig. 7c. (The phase speed of eigenmode $+ +0$ decreases, whereas that of eigenmode $+ +2$ increases as the eccentricity is increased.) Figure 8 shows the amplification rates and phase speeds of $+ +0$ and $+ +2$ modes as function of frequency. It is apparent from the figure that selection of frequency in the vicinity of the most amplified frequency does not alter the behavior of two modes described in Fig. 7c.

Under the in-phase forcing of the circular jet, the $m = 0$ mode [constant amplitude and phase along the aximuthal direction (see Fig. 3)] would be the dominating one. With similar reasoning, it is assumed that in-phase forcing of the jet selects out a linear combination of the fluctuation-of-velocity eigenmodes of the $+ +$ class (in the elliptic-core jet) or $c_{3\ell}$ class (in the triangular jet). The coefficients of eigenmodes can be found through biorthogonal relations.[7] Constructing a proper linear combination of the eigenfunctions of the two modes (actually another higher mode evolved from $m = 4$ is used) yields streamline patterns emanating from the minor and major axes, as shown in Fig. 9. The roll-up location of the major axis is clearly delayed slightly further downstream relative to that of the minor axis. This is demonstrated experimentally in the initial development region of a forced (in-phase) elliptic jet, as shown in Fig. 10. More details, such as the method of constructing the linear combination of eigenmodes, the effects of violating one of three condition owing to compressibility, and variation in azimuthal momentum thickness and temperature, are reported in Refs. 7 and 19. Needless to say, the behavior of eigenmodes c_0 and c_3 for U1 in the triangular-core jet displays remarkable similarities to that of eigenmodes of the elliptic-core jet. The behavior is represented by the polarized locations of the eigenfunctions and the creation of phase-speed difference without loss of comparable amplification rates between the eigenmodes. This suggests that roll-up of the portions of the triangular vortical structure around the vertices is slightly delayed further downstream relative to portions of the flat side in the triangular-core jet with U1. Thus, the rolled-up structure in the triangular shape appears to be deformed. The mechanisms for the deformations of the initial coherent structures in both noncircular jets (elliptic- and triangular-core jets) are found to be the same. These mechanisms will be discussed further in relation to the corresponding experiment results in the following section.

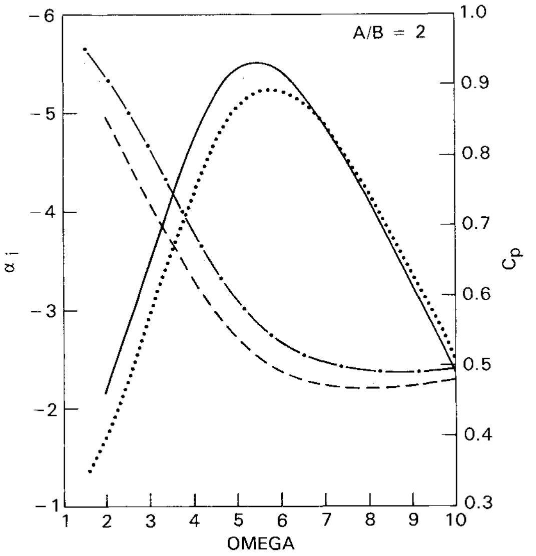

Fig. 8 α_i **(solid line for + +0 and dotted line for + +2) and** C_p **(dashed line for + +0 and chain-dotted line for + +2) are shown as functions of** ω**.**

The calculations of the velocity fluctuation eigenfunction for fundamental and overtone modes with NU1 show that the velocity fluctuations concentrate at the center section of the flat sides of the triangular jet and are absent from the vertices in the initial development region. In order to have deformation of the coherent structures in the triangular-core jet, it is suggested that an equal momentum thickness must be achieved in the flow development process. In the following section, these results are compared with experimental results obtained for various triangular configurations.

V. Experimental Results

Two different triangular jets were tested to study the effect of the initial momentum thickness distribution on the growth pattern of the jet. One jet has a triangular orifice nozzle, and the other was discharged from a triangular pipe.

The orifice nozzle has an equilateral triangular shape with an equivalent diameter of 50 mm. A bell-mouthed contraption is attached to the upstream section of the orifice to eliminate separation and to reduce the overshoot of the mean-velocity profile, typical in orifice jets. The nozzle is attached to the ducting system, which includes a settling chamber, screens, and honeycombs to reduce the turbulence level. At a Reynolds number of 40,000, the exit turbulence level is 0.4%. The initial momentum thickness at the flat side is equal to 0.0073 D_e, and that at the vertex side is 84% thicker.

A 40-W 12-in. loudspeaker is mounted in the settling chamber wall to apply forcing to the flow. The wavelengths corresponding to the forcing frequencies are more than an order of magnitude larger than the nozzle diameter. This implies that the forcing was predominantly in-phase (axisymmetric) and coherent. Flow visualization is done by direct photography of smoke injected into the jet's shear layers

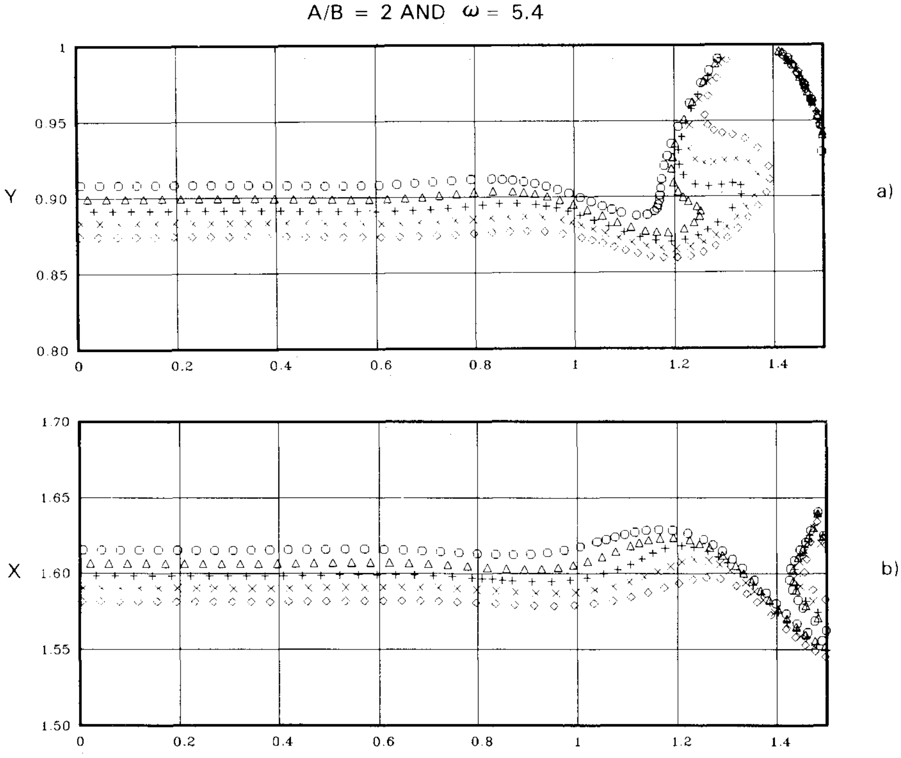

Fig. 9 Streakline patterns for elliptic-core jet in a) minor and b) major axis planes.

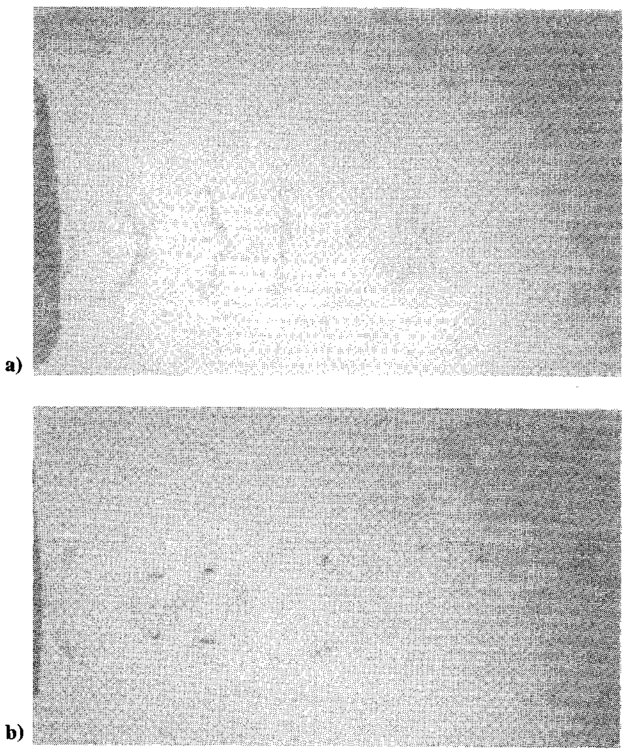

Fig. 10 Initial development region (indicated by *i*) and subsequent axis switching region (indicated by *s*) of a forced elliptic jet in a) minor and b) major axis planes.

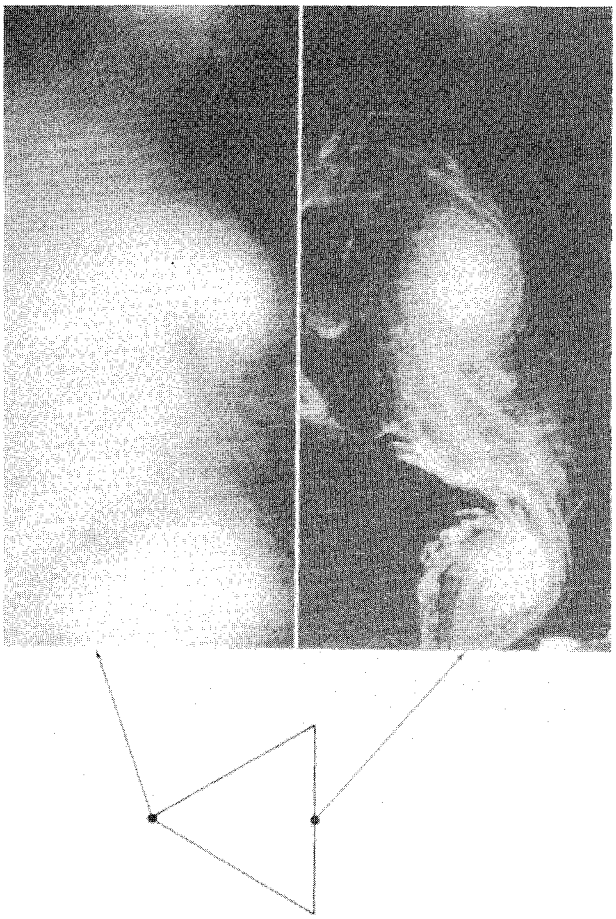

Fig. 11 Flow patterns of the equilateral-triangular jet issued from the center of the flat side and from the vertex, with forcing frequency at its preferred mode frequency.

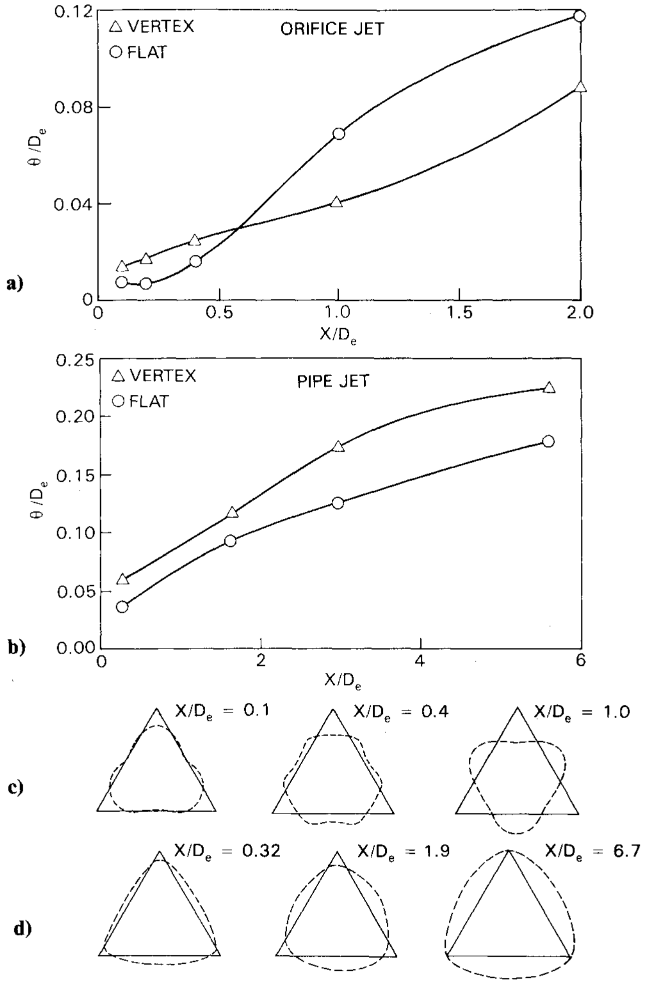

Fig. 12 Variation of the momentum thickness with the axial distance for the vertex and flat sides of the triangular jet, orifice jet, a), and pipe jet, b), and corresponding growth patterns of the contour, c) and d), respectively ($W = 0.5$ mean velocity represented by the dashed line), at various streamwise distances x/D_e.

through a 0.5-mm pipe. A strobe light synchronized with the jet's forcing signal is used to study the structures at different frequencies and phases relative to the forcing signal.

The pipe jet has an equilateral-triangular cross section, with an equivalent diameter of 19 mm, and is 19 diam long. The initial momentum thickness at the flat side is 0.047 D_e, and that at the vertex side is 70% thicker. The Reynolds numbers is 60,000, and the turbulence level at the exit is 4%. The mean and turbulent flowfield measurements are carried out using hot-wire anemometry with 50-kHz frequency response. The calibration, data acquisition, and analysis are done using a laboratory minicomputer.

The flowfield of the equilateral-triangular orifice jet is visualized by smoke in an airjet. Figure 11 shows the flow patterns of the jet at the center of the flat side and at the vertex for a jet that is excited at its preferred mode frequency. Large coherent structures are generated in the jet's shear layer at the flat side, whereas the shear layer at the vertex is turbulent with predominantly fine-scale eddies. The formation of coherent structures at the flat sides and their absence from the vertices correlate with the calculation results discussed in the previous section, showing that the activities of eigenfunctions with NU1 are concentrated at the flat sides.

The evolution of the momentum thickness in the streamwise direction is different for pipe and orifice jets. The initial momentum thickness is higher at the vertices relative to the flat sides for both jets. For the orifice jet, the momentum thickness of the vertex becomes the same as that of the flat side at a streamwise distance 0.6 D_e, as shown in Fig. 12a. Figure 12b shows that the momentum thickness at the vertex remains always greater than that of the flat side, even up to the streamwise distance of 6 D_e for the pipe jet.

The stability calculations discussed in the previous sections showed that, for NU1 (the momentum thickness at the vertex was greater than that at the flat side), all of the calculated instability modes were concentrated at the flat side. When U1 (equal azimuthal momentum thickness distribution) was achieved, the activities of one of the instability modes shifted to the vertex, whereas the other mode was predominantly concentrated at the flat side. It was also shown that there was no loss of comparable amplification rates and that phase-speed difference was created between two modes. These mechanisms led to the deformation of the initial coherent structures by the bending of the vertex sections in the streamwise direction. The deformation was followed by the completion of axis switching in the elliptic and triangular jets, as shown in Figs. 10 and 12c, respectively. In the case of the pipe jet, the axis switching was not observed, as seen in Fig. 12d, because the condition for the azimuthal momentum thickness distribution to be U1 was not achieved [see Fig. 12b)]; therefore, the mechanisms needed for the deformation and the axis switching did not exist.

VI. Concluding Remarks

The attempt was made to identify the underlying mechanisms for the deformation of the coherent structure that occurs in the initial stage of the axis switching of the noncircular jets. The generalized shooting method is applied to jets with elliptic- and equilateral-triangular-core regions of constant flow. The analysis shows three common behaviors of the eigenmodes in the noncircular jets having the deformation. These are 1) the eigenfunctions are properly localized without excessive overlapping; 2) the amplification rates of the corresponding eigenmodes are comparable; and 3) sufficient phase-speed difference exists between the eigenmodes. These conditions are satisfied in the triangular-core jet with U1, indicating that it is necessary to have an equal azimuthal momentum thickness distribution in order to have the deformation of the coherent structures. This theoretical finding is supported by the experimental investigation, which is carried out with the use of the orifice and pipe jets. The orifice jet shows U1 condition in the flow development proess, whereas U1 condition is not achieved in the case of the pipe jet. Consequently, the axis switching is observed in the orifice jet but not in the pipe jet. The initial development region of the orifice jet is described by NU1 condition, and the generations of the large-scale coherent structures at the flat side and turbulent, predominantly fine-scale eddies are found at the vertex. This is correlated with the theoretical results, which show that all of the eigenfunction activities are located at the flat side, with negligible activites found at the vertex with NU1 condition.

Acknowledgments

We wish to thank R. L. Derr for encouragement given us during the course of this work, C. M. Ho for helpful discussion and N. N. Mansour for providing access to the NAS Computer Facility, NASA Ames Research Center, Moffett Field, California. This was was supported by ONR. One of us (AT) wishes to acknowledge the American Society for Engineering Education for sponsoring his summer appointments (1985–1986) at the Naval Weapons Center.

References

[1] Browand, F. K., Chu, W. T., and Laufer, J., "Exploratory Experiments on the Entrance Effects in Subsonic Jet Flows," Univ. of Southern California, Los Angeles, CA, Rept. USCAE 130, 1975.

[2] Krothapalli, A., Baganoff, D., and Karamacheti, K., "On the Mixing of a Rectangular Jet," *Journal of Fluid Mechanics,* Vol. 107, 1981, pp. 201–220.

[3] Sfeir, A., "Investigation of Three-Dimensional Turbulent Rectangular Jets," AIAA Paper 78-1185, July 1978.

[4] Sforza, M. P., Steiger, M. H., and Trentacoste, N., "Studies on Three-Dimensional Viscous Jets," *AIAA Journal,* Vol. 4, May 1966, pp. 800–806.

[5] Trentacoste, N. and Sforza, M. P., "Further Experimental Results for Three-Dimensional Jets," *AIAA Journal,* Vol. 5, May 1967, pp. 885–891.

[6] Wlezien, R. W., and Kibens, V., "Passive Control of Jets With Indeterminate Origins," *AIAA Journal,* Vol. 24, Aug. 1986, pp. 1263–1270.

[7] Koshigoe, S., Tubis, A., and Ho, C. M., "Vortex Deformation in Elliptic-Core Jets from the Perspective of Instability Analysis," *Physics of Fluids,* Vol. 31, No. 9, 1988, pp. 2504–2517.

[8] Husain, H. S., and Hussain, A. K. M. F., "Control Excitation of Elliptic Jet," *Physics of Fluids,* Vol. 26, 1983, pp. 2763–2766.

[9] Ho, C. M. and Gutmark, E., "Vortex Induction and Mass Entrainment in a Small Aspect Ratio Elliptic Jet," *Journal of Fluid Mechanics,* Vol. 179, 1987, pp. 383–405.

[10] Gutmark, E., Schadow, K.C., Parr, D. M., Harris, C. K., and Wilson, K. J., "The Mean and Turbulent Structure of Noncircular Jets," AIAA Paper 85-0543, March 1985.

[11] Schadow, K. C., Gutmark, E., Parr, D. M., and Wilson, K. J., "Selective Control of Flow Coherence in Triangular Jets," *Experiments in Fluids,* Vol. 6, 1988, pp. 129–135.

[12] Gutmark, E., Schadow, K. C., Park, T. P., and Wilson, K. J., "Noncircular Jets in Combustion Systems," AIAA Paper 87-1379, June 1987.

[13] Schadow, K. C., Wilson, K. J., and Gutmark, E., "Reduction of Flow Coherence in Forced Subsonic Jets," AIAA Paper 85-1109, July 1985.

[14] Koshigoe, S. and Tubis, A., "Wave Structures in Jets of Arbitrary Shape. II. Application of a Generalized Shooting Method to Linear Instability Analysis," *Physics of Fluids,* Vol. 30, No. 6, 1987, pp. 1715–1723.

[15] Koshigoe, S. and Tubis, A., "Wave Structures in Jets of Arbitrary Shape. I. Linear Inviscid Spatial Instability Analysis," *Physics of Fluids,* Vol. 29, No. 12, 1986, pp. 3982–3992.

[16] Tinkham, M., *Group Theory and Quantum Mechanics,* McGraw-Hill, New York, 1984.

[17] Morris, P.J., "Instability of Elliptic Jets," *AIAA Journal* (to be published).

[18] Lichtenberg, A. J. and Liebermann, M. A., *Regular and Stochastic Motion,* Springer-Verlag, Berlin, 1983.

[19] Koshigoe, S., Ho, C. M., and Tubis A., "Application of a Generalized Shooting Method to the Linear Instability Analysis of Elliptic Core Jets," AIAA Paper 87-2733, Oct. 1987.